Design and development of plastic antibodies against SARS-CoV-2 RBD based on molecularly imprinted polymers that inhibit in vitro virus infection

ARTICLE

Design and Development of Plastic Antibodies against SARS-CoV-2 RBD based on Molecularly Imprinted Polymers that Inhibit *In Vitro* Virus Infection

Received 00th January 20xx,
Accepted 00th January 20xx

DOI: 10.1039/x0xx00000x

Ortensia Ilaria Parisi,[a,b] Marco Dattilo,†[a] Francesco Patitucci,†[a] Rocco Malivindi,[a,b] Serena Delbue,[c] Pasquale Ferrante,[c] Silvia Parapini,[d] Roberta Galeazzi,[e] Mariangela Cavarelli,[f] Francesco Cilurzo,[g] Silvia Franzè,[g] Ida Perrotta,[h] Vincenzo Pezzi,[a,b] Francesca Selmin,[g] Mariarosa Ruffo[a,b] and Francesco Puoci* [a,b]

The present research study reports the development of plastic antibodies based on Molecularly Imprinted Polymers (MIPs) able to selectively bind a portion of the novel coronavirus SARS-CoV-2 spike protein. Indeed, Molecular Imprinting represents a very promising and attractive technology for the synthesis of MIPs characterized by specific recognition abilities for a target molecule. Given these characteristics, MIPs can be considered tailor-made synthetic antibodies obtained by a templating process. After *in silico* analysis, imprinted nanoparticles were synthesized by inverse microemulsion polymerization and their ability to prevent the interaction between ACE2 and the receptor-binding domain of SARS-CoV-2 was investigated. Of relevance, the developed synthetic antibodies are able to significantly inhibit virus replication in Vero cells culture, suggesting their potential application in the treatment, prevention and diagnosis of SARS-CoV-2 infection.

Introduction

Severe Acute Respiratory Syndrome Coronavirus 2 (SARS-CoV-2) is the etiological agent of the current COVID-19 pandemic.[1] As of 3 June 2021, 171.222.477 confirmed cases, including 3.686.142 deaths, have been globally reported to WHO since the start of the outbreak.[2]

The genome of SARS-CoV-2 encodes four structural proteins: the spike protein, the envelope protein, the membrane protein, and the nucleocapsid protein. The coronavirus spike protein is a surface protein that mediates host recognition and attachment. It consists of two functional subunits: the S1 subunit, which contains a Receptor-Binding Domain (RBD) responsible for host cell receptor recognition and binding, and the S2 subunit, which is involved in the viral and host membranes fusion. These two processes, which represent the initial steps in the coronavirus infection cycle, are crucial in determining host specificity, tissue tropism and transmission capacity.[3, 4]

Although the SARS-CoV-2 genome is closer to bat-SL-CoVZC45 and bat-SL-CoVZXC21 than SARS-CoV (about 79% similarity) and MERS-CoV (about 50% similarity),[5] the RBD structure presents a high homology to that of SARS-CoV and both viruses use angiotensin-converting enzyme 2 (ACE2) as host cell receptor.[6-8] Both SARS-CoV and SARS-CoV-2 belong to the β-genus and the overall sequence similarities between SARS-CoV-2 and SARS-CoV spike proteins are around 76%-78% for the whole protein and around 73%-76% for the RBD.[7] Therefore, the spike protein, playing a key role in human-to-human transmission of this novel coronavirus,[1, 9, 10] represents the primary target for the development of antibodies, vaccines, therapeutics and diagnostic agents.

Due to the urgent need to control the coronavirus disease 2019 pandemic, the research attention is focused on the development of drugs and vaccines able to treat and prevent SARS-CoV-2 infection, respectively.

Currently, the U.S. Food and Drug Administration (FDA) has authorized three COVID-19 vaccines for emergency use.[11] On December 11, 2020, FDA approved the first emergency use authorization (EUA) for the Pfizer-BioNTech vaccine for the prevention of COVID-19 caused by SARS-CoV-2 in individuals 16 years of age and older.[12] This vaccine contains a nucleoside-modified messenger RNA (modRNA) encoding the spike protein of SARS-CoV-2 formulated in lipid particles. On December 18, 2020, FDA issued an emergency use authorization for the second vaccine, such as the Moderna COVID-19 Vaccine, which

[a] *Department of Pharmacy, Health and Nutritional Sciences, University of Calabria, 87036 Rende (CS), Italy.*
[b] *Macrofarm s.r.l., c/o Department of Pharmacy, Health and Nutritional Sciences, University of Calabria, 87036 Rende (CS), Italy.*
[c] *Department of Biomedical, Surgical and Dental Sciences, Laboratory of Translational Research, University of Milan, 20133 Milano, Italy.*
[d] *Department of Biomedical Sciences for Health, University of Milan, 20133 Milan, Italy.*
[e] *Department of Life and Environmental Sciences, Marche Polytechnic University, 60131 Ancona, Italy.*
[f] *Université Paris-Saclay, Inserm, CEA, Center for Immunology of Viral, Auto-immune, Hematological and Bacterial diseases (IMVA-HB/IDMIT), Fontenay-aux-Roses & Le Kremlin-Bicêtre, France.*
[g] *Department of Pharmaceutical Sciences, University of Milan, 20133 Milan, Italy.*
[h] *Department of Biology, Ecology and Earth Sciences, University of Calabria, 87036 Rende (CS), Italy.*
† These authors contributed equally.
Electronic Supplementary Information (ESI) available: [details of any supplementary information available should be included here]. See DOI: 10.1039/x0xx00000x

is also based on the mRNA technology and can be now distributed in the U.S. for use in individuals 18 years of age and older.[13] The third vaccine to obtain emergency use approval by FDA was the Janssen COVID-19 Vaccine on February 27, 2021.[14] This vaccine uses a viral vector, such as the adenovirus type 26 (Ad26), to deliver a piece of DNA encoding for the SARS-CoV-2 spike protein. After the vaccine injection, the body is temporarily able to assemble spike proteins, which are recognized by the immune system producing an immune response against SARS-CoV-2.

Among the most explored strategies for the identification of potential COVID-19 therapeutics, the use of repurposed drugs and the development of monoclonal antibodies targeting specific sites of vulnerability of the spike protein play a key role.[15-17] As of June 3, 2021, nine treatments for COVID-19 and serious conditions caused by this coronavirus disease are currently authorized for emergency use and only one treatment is currently approved by the FDA for use in COVID-19 such as the antiviral drug Veklury (remdesivir).[18] Despite Veklury represents the first treatment for COVID-19 to receive FDA approval for use in adult and pediatric patients 12 years of age and older requiring hospitalization, monoclonal antibodies are receiving considerable attention due to their ability to neutralize SARS-CoV-2. At this time, some monoclonal antibodies under investigation for the treatment of COVID-19, and not currently approved for any indication, achieved the Emergency Use Authorization by FDA. These antibodies are able to target and bind the receptor-binding domain of SARS-CoV-2 spike protein and obtained the authorization for emergency use for the treatment of mild to moderate COVID-19 in adults and pediatric patients (12 years of age and older weighing at least 40 kg), who are at high risk for progressing to severe COVID-19 and/or hospitalization.[19]

However, traditional antibodies present several drawbacks such as limited stability, unsuitable pharmacokinetics, inefficient tissue penetration and impaired interactions with the immune system.[20, 21] Last but not least, conventional antibodies require high production costs and suffer from ethical issues in *in vivo* tests on animals.[22]

An interesting alternative consists of synthetic antibodies made by polymers. In this context, Molecular Imprinting represents a very promising and effective technology for the preparation of polymeric matrices characterized by receptor-like properties.[22, 23] Molecularly Imprinted Polymers (MIPs), indeed, are synthesized by polymerizing functional and crosslinking monomers around a target molecule called template and their selective recognition abilities are due to the formation of a complex between the target analyte and the selected functional monomers during the pre-polymerization step.[24, 25] Moreover, being synthetic materials, MIPs are robust, physically and chemically stable in a wide range of conditions including temperature and pH, and more easily available due to a low-cost, reproducible and relatively fast and easy preparation compared to the biological counterpart.[26, 27] Therefore, this kind of materials combines the robustness of polymers with the selectivity of natural receptors finding potential application in the field of antibody mimics. In addition, MIPs are characterized by significant versatility[28] and can be designed and engineered according to their specific application developing polymers with magnetic and/or fluorescent properties, for instance.

Several studies report on MIPs for targeting glycans and protein-based cell receptors that are overexpressed in specific diseases including tumors.[29] When loaded with therapeutic agents, indeed, these polymeric materials can act as drug delivery systems able to accumulate in tumor and, thus, release the drug at the site of action. In addition, MIPs can also be used as free-drug therapeutics able to counteract tumor growth. Medina Rangel et al. developed MIPs selective for cadherins, which are transmembrane proteins mediating cell-cell adhesion and involved in tumor progression and metastasis, able to inhibit cancer cell invasiveness *in vitro* and disrupt tumor spheroids.[30] Another interesting study describes MIPs able to bind HER2 glycans and, thus, to block the signaling pathway of this receptor inhibiting breast cancer growth.[31]

Moreover, Molecular Imprinting Technology allows to prepare MIPs-based synthetic antibodies able to recognize and bind different microorganisms including bacteria and viruses.[23] In literature, several examples of virus-imprinted polymers were reported for the development of biosensors for the detection of infectious diseases caused by these microorganisms, including Dengue virus, Japanese encephalitis virus (JEV), human immunodeficiency virus (HIV), hepatitis A virus, hepatitis B virus, adenovirus, and picornaviruses.[32, 33] On the contrary, only few works are focused on the application of virus-imprinted polymers as synthetic neutralizing antibodies. Recently, Graham et al. developed a hydrogel-based MIP using porcine reproductive and respirator syndrome virus (PRRSV-1) as a model mammalian virus demonstrating its effective virus neutralization capacity.[34]

The aim of the present study was to develop plastic antibodies based on Molecularly Imprinted Polymers for the selective recognition and binding of SARS-CoV-2 RBD in order to block the function of the spike protein. Alternative pharmacological approaches, indeed, can potentially be used for the delivery of MIPs-based antibodies as prophylaxis strategy to prevent infection and as treatment of SARS-CoV-2 positive patients in order to inhibit viral replication in the early phase of infection.

Results and discussion

Molecular Docking Studies

A computational approach to allow the rational selection of an appropriate monomer for Molecularly Imprinted Synthetic Material Antibodies (MISMAs) selectively rebinding SARS-CoV-2 spike protein in its RBD domain has been carried out. Molecular docking combined with quantum chemical calculations was used for modeling and comparing different monomers affinity and their ability to polymerize onto the RBD portion of the Spike protein, thus preventing its binding to ACE2 receptor.

As it is known, the considerable amount of different functional groups present in the target protein creates potential premises for multiple non-covalent interactions (H-bond, van der Waals,

electrostatic, and/or hydrophobic) between the protein and functional monomers in a pre-polymerization complex before MIP synthesis. It can be assumed that these interactions are to some extent maintained during the polymerization and play a crucial role in the formation of complementary binding sites after the template protein removal, which is necessary for the subsequent selective rebinding of the target protein to the MIP. Consequently, an estimation of all possible non-covalent interactions binding sites as well as their strength in the protein-monomer complex must be taken into account in order to design MIPs targeting specific proteins with highly selective recognition sites (i.e. high specificity). Using a molecular modeling approach, the aim here was to compare the capability of different functional monomers for building a polymer with macromolecular imprints capable of selectively rebinding protein-sized analytes.

Molecular docking was applied to find both energetically favorable binding poses of the selected functional monomer on the model protein and to predict the probable arrangement of multiple monomer molecules around the macromolecular target. A particular attention has been put in partial charges calculation on the functional monomers since the small dimension of the molecules considered (acrylamide and acrylic acid) will allow them to easily bind on the protein target surface, and the electron density and charge distribution are primary responsible for the electrostatic/hydrophobic non-covalent complex stabilization.

The approach was based on using the docking of each of the monomers throughout all the RBD surface to determine the energetically favorable binding poses and, finally, to assess the cumulative strength of H-bond interactions between the monomers and the sterically accessible proton-acceptor groups of RBD, such as polar amino acids.

Acrylamide Docking Results. The results obtained from the docking of acrylamide (using both mk then nbo charges) identified a close clusters' distributions. We excluded those poses that are not accessible to the SAS (Solvent Accessible Surface) surface or that lie at the interface between monomers in the trimeric spike protein association (pdb code 6vsb), and we observed that only clusters reporting poses on the RBM (Receptor-Binding Motif) portion of the RBD domain remains (Fig. 1A).

As shown in Fig. 1B, they are equally distributed around the six key residues interacting with ACE2 receptor.[35]

The cluster population is cl5 (25%) (dark purple), cl6 (19%) (dark green), cl7 (25%) (gold), cl8 (12%) (cyan), cl9 (13%) (orange), 10 and 11 (0.03%) (violet and blue). The cluster cl 1-4 are those excluded since they are not significantly populated and lie in not accessible zones on the whole protein surface. This over-spread distribution, together with a comparable population percentage, and comparable binding energy suggest that this monomer can efficiently bind and select the RBM portion of the target protein occupying positions that can efficiently lead to the polymerization process.

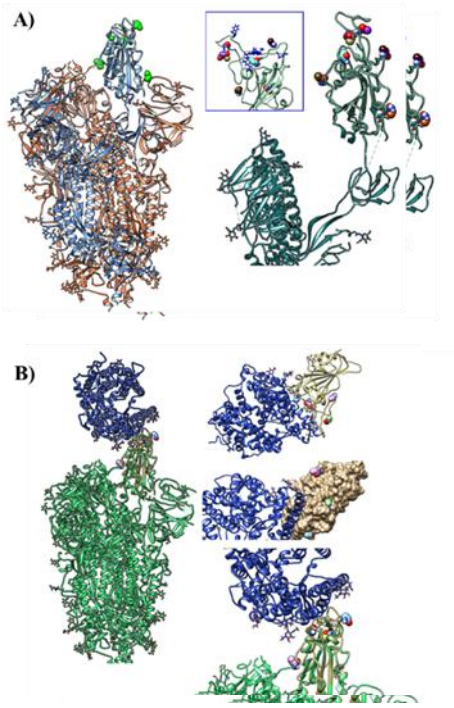

Figure 1. Molecular docking images. PANEL A: Left) 6vsb trimeric spike protein, blue chain A (RBD up conformation), coral chains B-C (RBD down conformation), in association with functional monomer acrylamide (green spheres) in its populated docked clusters. **Right)** acrylamide clusters distributions accessible to solvent surface on RBD domain of the spike protein (6vsb). **Top right)** In blue are highlighted the 6 key residues implicated in ACE2 binding (residues 417,455, 486 493,494, 501). **Down right)** same, less magnified; **PANEL B: Left)** trimeric form of the spike protein (6vsb) (green) in complex and significative clusters poses for functional monomer acrylamide (wan der Waals spheres) with ACE2 binding domain (blue); RBD domain in the up conformation is represented as gold ribbons. **Right)** spike protein RBD domain in complex with ACE2 receptor (6m0j) and significative clusters poses for functional monomer acrylamide (wan der Waals spheres) (top) Ribbons (middle) RBD as molecular surface (b) Zoom on ribbons is shown.

Acrylic Acid Docking Results. The results obtained from the docking of acrylic acid showed mainly the existence of four accessible clusters with high population spread all over the RBD surface. Two of these four clusters (namely cl1 and cl3) are near even not so close to the RBM-6 residues (Fig. 2A), while the other two lie exactly within the RBM portion and both interact with some of the 6 residues.

In particular, the fourth cluster pose (cl4) is stabilized by a strong electrostatic interaction involving the positive charged Lys417 lateral chain and the carboxylate moiety of acrylic acid (Fig. 2B).

This distribution of the docked clusters together with the high population found out, suggests that this monomer is perfectly suitable to be considered as a promising monomer for targeted polymerization. In order to take into account the acrylic acid partial dissociation at physiological conditions (pKa = 4.26), a molecular docking study has been carried out also for its conjugate base (acrylate).

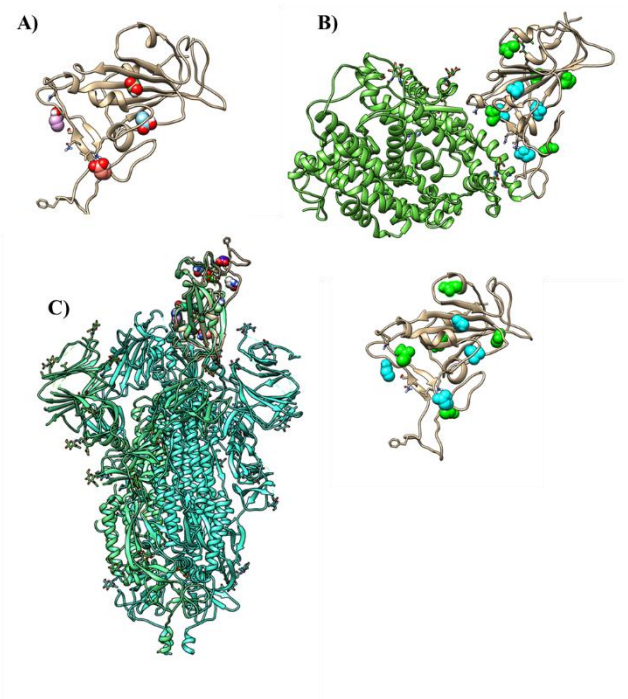

Figure 2. Molecular docking images. PANEL A: RBD domain of the spike protein in complex with acrylic acid, as Van der Waal spheres (violet cl2, salmon cl4 (in RBM), cyan cl1 and green cl3); **PANEL B:** RBD domain of the spike protein in complex with the ACE2 receptor (6m0j) and significative clusters poses for functional monomers acrylic acid (cyan as van der Waals spheres) and acrylamide (green, van der Waals spheres). The 6 key residues implicated in ACE2 binding (namely 417, 455, 486, 493, 494, 501) are represented with the lateral chains at the proteins' interface; **PANEL C:** Spike protein in its open active conformation (pdb code 6vyb), trimeric form (ribbons light green; the lighter green ribbons correspond to the protein chain carrying RBD domain in the open con-formation); acrylic acid and acrylamide populated docked clusters to its RBD are reported together (var der Waals spheres representation).

As a result, we obtained the same cluster organization observed for acrylic acid and, thus, we can state that the pH values cannot invalidate the acrylic acid affinity since it has the same high affinity both in its undissociated and dissociated molecular forms.

The obtained results clearly indicate that both acrylamide and acrylic acid monomers can gain the chance to bind and polymerize on the RBD surface. However, their overall distribution suggest that their positioning is perfectly complementary since they cover different zones of the RBD surface (Fig. 2B,C). For this reason, we expect that their combined use might guarantee a major specificity (acrylic acid binds directly one of the RBM-6 residues) and major strengths.

Other Monomers Docking Results. Following the same protocol reported in the methods/computational results section, we performed molecular docking calculation on other currently used monomers, i.e. N-isopropylacrylamide (NIPAm), N-tert-butylacrylamide (TBAm), N-(3-aminopropyl)methacrylamide hydrochloride (NAPMA), in order to evaluate the feasibility of their usage as MIPs monomers.

From the collected results, all these three monomers showed a very similar behavior.

More in details, TBAm showed the existence of only two clusters, the first being significatively more populated (>80%) and positioned far away the RBM portion of RBD; the second cluster is much lower in energy and is still positioned far from N501 (Fig. 3A). NIPAm monomer showed the presence of only one cluster at low energy with population higher than 85% but located far from RBM (Fig. 3B); finally, NAPMA has for clusters populated and close in energy (overall population >90%), no cluster is located near and around the RBM region, but they are positioned at the opposite site (Fig. 3C). These results exclude the possibility of consider these monomers suitable for MIPs targeting RBD.

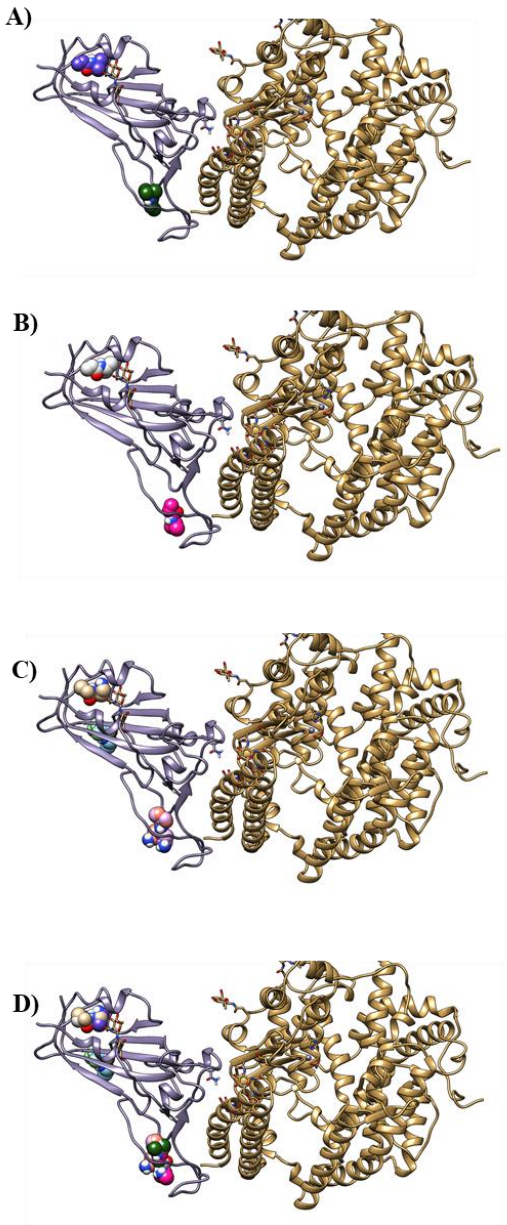

Figure 3. Spike protein RBD domain (violet ribbons) in complex with ACE2 receptor (gold ribbons) (6m0j) and significative clusters poses for functional monomers TBAm (**PANEL A**), NIPAm (**PANEL B**) and NAPMA (**PANEL C**) (represented as van der Waals spheres); N501 is represented at the interface with its lateral chain. (**PANEL D**) All the three monomers are represented.

Synthesis of Molecularly Imprinted Synthetic Material Antibodies (MISMAs) and their Characterization

In literature, several studies report on MIPs able to recognize biomacromolecules, including proteins and viral components but also entire viruses.[36-40] Most of these works are focused on the development of sensors for the detection of these targets; on the contrary, only few of them investigate the therapeutic application of MIPs.[41] Here, we report the preparation of plastic antibodies consisting of tailor-made polymeric imprinted nanoparticles, which represent an alternative to the expensive traditional antibodies often unreliable due to their restricted stability.[21, 41] The synthetic antibodies based on MIPs were produced by inverse microemulsion polymerization according to the non-covalent imprinting approach.[42, 43]

Based on the results obtained by molecular docking, two different imprinted materials, namely $MISMA_1$ and $MISMA_2$, were synthesized using acrylamide and a mixture of acrylamide and acrylic acid as functional monomers, respectively.

The aqueous phase consisted of SARS-CoV-2 RBD and functional and crosslinking monomers, while the oil phase involved Tween 80 and Span 80 as emulsifier system dissolved in hexane. The water phase was added dropwise to the oil phase under stirring and, then, the polymerization was started at room temperature adding ammonium persulfate (APS) and N,N,N,N-tetramethylethylenediamine (TEMED). Non-Imprinted Polymers (NIPs) were also synthesized following the same experimental conditions, but in the absence of SARS-CoV-2 RBD. Reaction yields for MIPs and NIPs synthesis ranged from 78 to 83%.

The choice of the monomers represents a crucial point in the preparation of effective MIPs and it is based on their ability to establish interactions with the functional groups of the template molecule in a covalent or non-covalent way. Three main approaches, indeed, can be used to synthesize this kind of polymers depending on the nature of the interactions occurring between the template and the chosen functional monomers during both pre-polymerization and binding steps.[44] In the covalent one, template and functional monomers are covalently bound during the pre-polymerization phase and, after the polymerization reaction, the analyte is extracted from the polymeric matrix by chemical cleavage of the covalent bonds. Then, the same covalent interactions are re-formed during the rebinding. The semi-covalent approach involves the formation of covalent interactions during the polymerization process and non-covalent interactions in the rebinding step. Finally, the non-covalent approach is based on the formation of non-covalent interactions, including hydrogen bonds and electrostatic, π-π and hydrophobic interactions, between template and monomers during the polymerization process and the subsequent recognition phase. This method is widely employed due to several advantages such as the simple experimental procedure and the large variety of appropriate functional monomers.

In the present study, the last imprinting approach was chosen for the MIPs-based antibodies preparation due to the nature of the template-monomers interactions, which are similar to those found in biological systems. The choice of the adopted functional monomers was based on the results obtained by *in silico* studies, which play a key role in optimizing polymer composition to prepare high-affinity materials.

Once the polymerization reaction has taken place, the template is extracted leading to a porous crosslinked polymeric matrix containing binding holes fitting size, shape and functionalities of the target compound.

TEM images (Fig. 4A) highlight that both MISMAs present an irregular shape and an almost porous structure.

Particle size distribution of MISMAs as evidenced by both DLS (Fig. 4B) and NTA (Fig. 5) confirmed that the size of both MISMA nanoparticles was around 60-70 nm even if they had the tendency to form dimeric or multimeric structures despite their negative surface charge (-16.4 ± 0.36 and -18.3 ± 2.02 for $MISMA_1$ and $MISMA_2$, respectively).

In particular, in the case of $MISMA_1$ two main populations at less than 100 nm (Table 1) and two others exactly centered at double values (i.e. 125 nm and 200 nm) were observed. These values are compatible with the hypothesis of the formation of dimers. This trend was more evident in the case of $MISMA_2$ where single nanoparticles represent less than 1% of the whole population (Table 1).

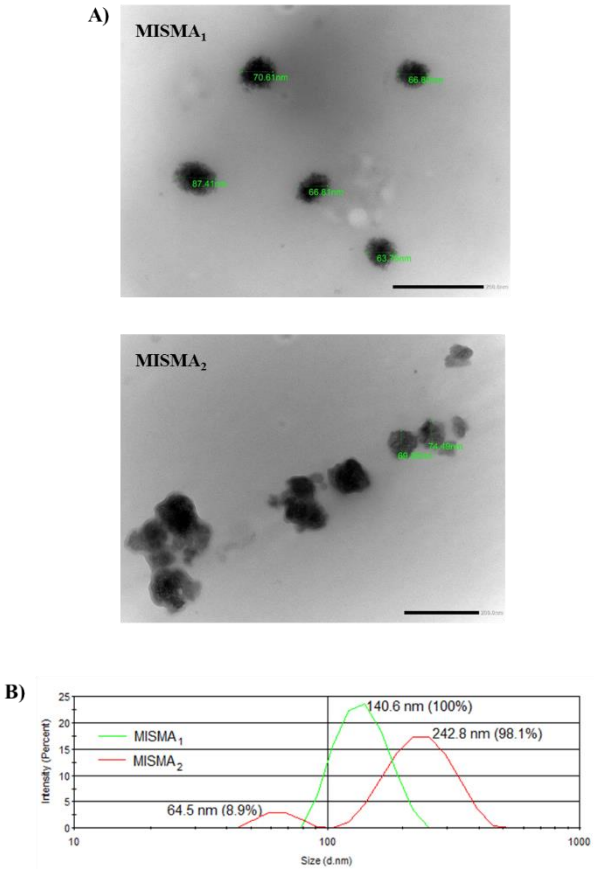

Figure 4. Morphology and particles size and distribution assessment. PANEL A: TEM micrographs of $MISMA_1$ and $MISMA_2$; **PANEL B:** DLS analysis of $MISMA_1$ and $MISMA_2$.

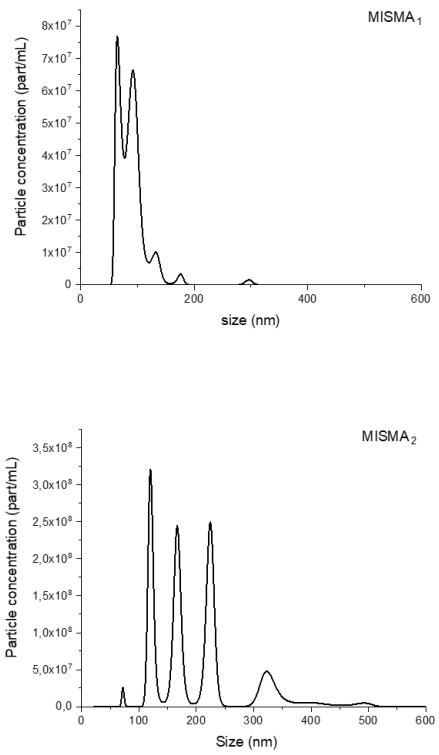

Figure 5. Exemplification of the NTA pattern of MISMAs.

Table 1. Percentage of MISMA single nanoparticles and multimers calculated on the bases of NTA traces (N=3).

	$MISMA_1$		$MISMA_2$	
	Size (nm)	**Area (%)**	**Size (nm)**	**Area (%)**
Single nanoparticle$_1$	68 ± 3	30.4 ± 1.3	66 ± 3	0.70 ± 0.28
Single nanoparticle$_2$	90 ± 3	50.9 ± 1.2	-	-
Dimer$_1$	125 ± 7	16.9 ± 9.0	118 ± 7	22.20 ± 5.52
Dimer$_2$	203 ± 4	1.4 ± 0.6	-	-
Multimers (sum of other peaks)			-	76.00 ± 6.55

The higher aggregation of $MISMA_2$ compared to $MISMA_1$ was also confirmed by the TEM images, which showed the presence of aggregates (Fig. 4A) and by particle concentration data, since $MISMA_1$ presented a higher number of nanosized particles with respect to $MISMA_2$ per equal polymer concentration ($MISMA_1$: $7.8x10^9$±$7.3x10^8$ particles/mL; $MISMA_2$: $1.5x10^9$±$5.4x10^7$ particles/mL).

Evaluation of the Imprinting Effect and Selectivity

In order to investigate both recognition properties and selectivity of the prepared imprinted polymeric nanoparticles, binding studies were carried out in phosphate buffer solution (PBS) at pH 7.4.

The imprinting effect was evaluated by binding experiments in which amounts of imprinted and non-imprinted nanoparticles were incubated with a standard solution of the SARS-CoV-2 receptor-binding domain. SDS-PAGE Electrophoresis was used to quantify the interaction of MISMAs with the novel coronavirus RBD. The obtained results highlighted the capability of both the prepared imprinted polymers to recognize and bind a higher amount of the target molecule compared to the corresponding non-imprinted ones (Fig. 6 and Table 2).

In particular, when imprinted nanoparticles were synthesized using a mixture of acrylamide and acrylic acid, the percentage of bound SARS-CoV-2 RBD was greater than that observed for imprinted nanoparticles prepared using acrylamide alone.

The same experimental conditions were adopted to perform selectivity studies, which involved a standard solution of a molecule structurally similar to the SARS-CoV-2 RBD such as the RBD of the SARS-CoV spike protein. The obtained results showed no significant differences between MISMAs and NIP nanoparticles in the interaction with SARS-CoV RBD (Table 2), confirming the specific and selective abilities of the imprinted polymers. These MISMAs properties, indeed, are due to the presence of selective molecular recognition holes that are complementary to the target template in terms of size, shape and functional groups. The choice of the functional monomer plays a key role in the imprinting process to ensure the formation of selective binding sites within the polymeric matrix. In this work, acrylamide and acrylic acid were chosen in the aim to promote both hydrophobic and electrostatic interactions with the receptor-binding domain of the novel coronavirus.

The imprinting factor (IF) and the selectivity coefficient (ε) were also calculated. The first parameter is the ratio between the amount of template, or its analogue, adsorbed by imprinted and non-imprinted nanoparticles respectively, while the second one is the ratio between the amount of SARS-CoV-2 RBD and the amount of SARS-CoV RBD adsorbed by MISMAs.[25] The imprinting factor IF represents a measure of the strength of interaction between imprinted polymer and template and the achieved values for the prepared $MISMA_1$ and $MISMA_2$ were 5.87 and 5.56, respectively, which are indicative of relevant adsorption abilities compared to the corresponding non-imprinted materials. Moreover, the calculated selectivity coefficients equal to 10.23 and 25.85 confirmed the selective binding properties of the developed synthetic antibodies.

Table 2. Percentages of bound SARS-CoV-2 receptor-binding domain and SARS-CoV receptor-binding domain by imprinted ($MISMA_1$ and $MISMA_2$) and non-imprinted (NIP_1 and NIP_2) nanoparticles. Data are shown as means ± S.D.

ANALYTE	**BOUND ANALYTE (%)**			
	$MISMA_1$	**NIP_1**	**$MISMA_2$**	**NIP_2**
SARS-CoV-2 RBD	44.0 ± 1.3	7.5 ± 0.7	51.7 ± 1.0	9.3 ± 1.1
SARS-CoV RBD	4.3 ± 0.6	4.6 ± 0.6	2.0 ± 0.8	0.1 ± 1.5

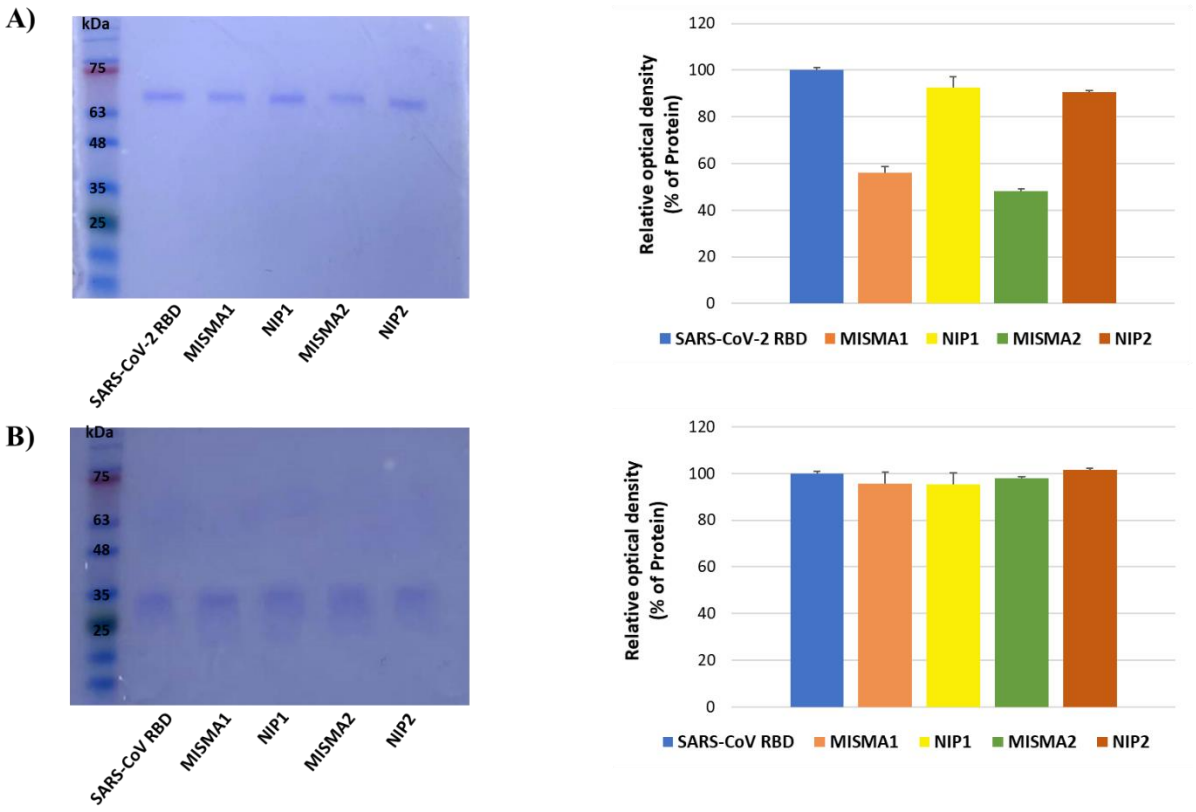

Figure 6. Binding Studies. SDS-PAGE Electrophoresis (Coomassie blue stained): **PANEL A)** SARS-CoV-2; **PANEL B)** SARS-CoV.

Dot-blot Assay

A dot-blot assay was carried out in the aim to further investigate the ability of the developed MISMAs to recognize and bind small amounts of the SARS-CoV-2 receptor-binding domain spotted on a nitrocellulose membrane. This assay allows to study also the sensitivity of the prepared synthetic antibodies and to determine a limit of detection.

As shown in Fig. 7A, unlike the corresponding non-imprinted nanoparticles, $MISMA_2$ were able to interact with different SARS-CoV-2 RBD concentrations with a detection limit of 1 ng.

Moreover, the performed dot-blot assay confirmed the specificity of the synthetic antibodies, which had no reactivity with a structural analogue such as the receptor-binding domain of SARS-CoV (Fig. 7B).

Adsorption Isotherms Studies

In order to better explore the nature of the interaction between the receptor-binding domain of SARS-CoV-2 and the synthesized plastic antibodies, $MISMA_2$ and the corresponding NIP_2 nanoparticles were incubated for 18 h with RBD standard solutions at different concentrations and, then, adsorption isotherms (Fig. 8) were obtained by plotting the amount of RBD adsorbed onto the two polymeric materials at equilibrium (Q_e, mg/g) versus C_i (µg/mL), which is the initial RBD concentration in solution.

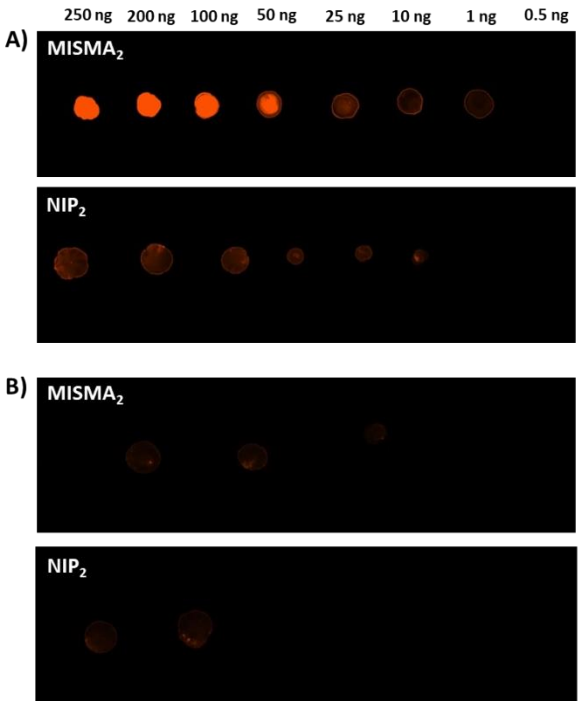

Figure 7. Dot-blotting analysis. PANEL A: different amounts of SARS-CoV-2 RBD were dropped on a nitrocellulose membrane and incubated with $MISMA_2$ and the control material NIP_2; **PANEL B:** different amounts of SARS-CoV RBD were dropped on a nitrocellulose membrane and incubated with $MISMA_2$ and the control material NIP_2.

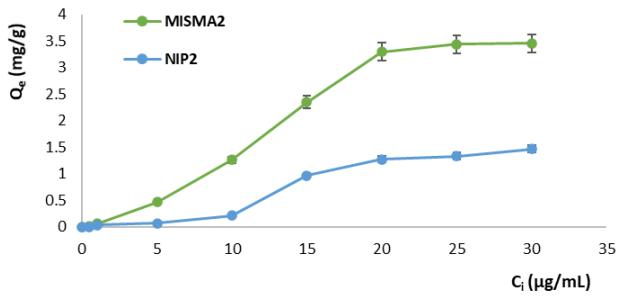

Figure 8. Adsorption isotherms of $MISMA_2$ and the corresponding NIP_2 upon incubation with RBD standard solutions at different concentrations.

As it is possible to observe in Fig. 8, with the increase of RBD C_i, the amount of the adsorbed protein initially grows until achieves saturation. Moreover, the maximum adsorption capacity of $MISMA_2$ (3.46 mg/g) is higher than that of the corresponding NIP_2 polymeric nanoparticles (1.47 mg/g) under the same experimental conditions, which is indicative of the recognition properties of the imprinted plastic antibodies.

The collected data were also analyzed using the Langmuir and Freundlich models, which are described by the following Equations (1 and 2), respectively:

$$\frac{1}{Q_e} = \frac{1}{Q_{max} C_e K_L} + \frac{1}{Q_{max}} \qquad (1)$$

$$\log Q_e = \log K_F + m \log C_e \qquad (2)$$

where Q_e is the amount of RBD bound per gram of polymeric nanoparticles at the equilibrium (µg/g), C_e is the protein equilibrium concentration (µg/mL), Q_{max} is the maximum adsorption capacity (µg/g), K_L is the Langmuir constant, K_F is the Freundlich constant and m is the heterogeneity index.

The Langmuir model assumes that a monolayer adsorption occurs on a uniform polymer surface characterized by the presence of a limited number of homogeneous binding sites, which are also equivalent in terms of energy and have the same binding capability. Therefore, the maximum adsorption is gained when the polymeric surface reaches saturation.[45] On the contrary, the Freundlich model describes a non-ideal adsorption process on a heterogeneous surface and not limited to the formation of a monolayer.[46]

Langmuir and Freundlich isotherms were obtained by plotting $1/Q_e$ versus $1/C_e$ and $\log Q_e$ versus $\log C_e$, respectively, and the fitting parameters were reported in Table 3.

Table 3. Fitting parameters for Langmuir and Freundlich isotherms.

POLYMER	LANGMUIR MODEL			FREUNDLICH MODEL		
	K_L	Q_{max}	R^2	K_F	m	R^2
$MISMA_2$	0.238	204.08	0.9424	137.44	1.6394	0.8787
NIP_2	0.108	114.94	0.8534	20.28	1.3985	0.9149

Based on the correlation coefficient values (R^2), the performed adsorption isotherm studies showed the best fit with Langmuir model, which was more suitable than the Freundlich one to describe the binding behaviour of the developed plastic antibodies. Therefore, these data confirmed the presence of homogeneous binding sites for the receptor-binding domain of SARS-CoV-2 onto the imprinted nanoparticles.

In vitro evaluation of MISMAs ability to inhibit ACE2–SARS-CoV-2 RBD interaction

In order to further confirm the ability of MISMAs to bind the SARS-CoV-2 RDB and, thus, inhibit its interaction with ACE2 receptor, an inhibitor screening assay kit was used. This kit is characterized by a high sensitivity of detection of mFc-tagged Spike protein (RBD) by HRP-labeled anti-mouse-Fc.

Imprinted and non-imprinted polymeric nanoparticles were tested at different concentrations in the range from 0.1 to 50 ng/µL and the achieved results (Fig. 9A) confirmed the capability of the developed plastic antibodies to reduce the binding of RBD to its receptor ACE2 in a concentration-dependent manner. On the contrary, no inhibition of the ACE2–SARS-CoV-2 RBD interaction was observed at any tested NIP_1 and NIP_2 concentration.

In addition, the collected data were used to calculate the amount of SARS-CoV-2 RBD bound to the polymers. Fig. 9B shows the binding isotherms of 1 ng/µL SARS-CoV-2 RBD to MISMAs and NIPs, which confirmed that MISMAs were able to bind more template than the corresponding non-imprinted nanoparticles. This suggests the presence of high affinity holes within the imprinted polymeric matrices that are absent in the NIP materials.

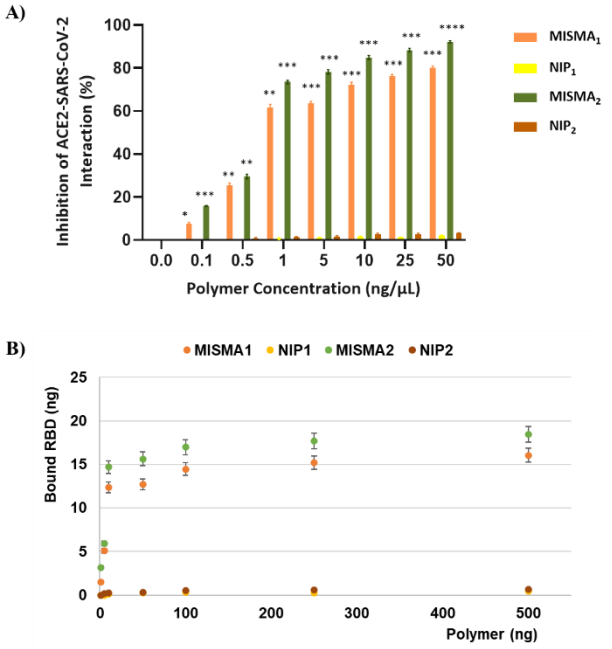

Figure 9. Inhibitor screening assay. PANEL A: Inhibition of ACE2-SARS-CoV-2 RBD interaction. The mean and SD of triplicates are shown. Significance of difference from control: *p < 0.05, **p < 0.01, ***p < 0.001 and ****p < 0.0001 as calculated with two-way ANOVA followed by Šídák's multiple comparison test. **PANEL B**: binding isotherms of 1 ng/µL SARS-CoV-2 RBD template to imprinted and non-imprinted nanoparticles.

MISMA$_1$ and MISMA$_2$ inhibit *in vitro* infection by authentic SARS-CoV-2 virus

Inhibition of SARS-CoV-2 viral replication by MISMAs was evaluated in Vero cells exposed to a viral isolate purified from a SARS-CoV-2 infected patient. In a preliminary experiment, cells were infected in absence and presence of MISMAs at concentrations ranging between 10 et 500 ng/µL. Those concentrations corresponded to a different number of particles according to the polymer used and included between 0.29 ± 0.02 and 39.2 ± 7.3 x 10^8 particle/mL (Table 4).

Virucidal studies taking into account the effect of NIP nanoparticles, used as control material, were also carried out.

Viral replication was quantified in the culture supernatant 72h post-infection by real-time RT-PCR and an inhibition curve was generated (Fig. 10A). MISMA$_2$ concentration below 100 ng/µL efficiently inhibit viral growth, with the maximum effect of 99 ± 0.5 % of inhibition observed with 20 ng/µL of the polymeric nanoparticles (Fig. 10 A,B).

Table 4. Tested MISMAs concentrations.

Concentration (ng/µL)	Particle x 10^8/mL*	
	MISMA$_1$	MISMA$_2$
10	0.8 ± 0.1	0.29 ± 0.02
20	1.6 ± 0.3	0.58 ± 0.02
30	2.4 ± 0.4	0.87 ± 0.03
100	7.8 ± 1.5	2.90 ± 0.27
250	19.6 ± 3.6	7.26 ± 0.27
500	39.2 ± 7.3	14.5 ± 0.54

*measured by NTA

On the contrary, a clear dose-response effect was not observed in presence of MISMA$_1$ (Fig. 10A). Moreover, no virucidal activity was observed for the non-imprinted polymers (Fig. 10A) confirming that the nanoparticles themselves are not able to cause a viral inhibitory effect.

To confirm these results, a plaque reduction assay was optimized for testing the potential inhibitory effect on virus infectivity of MISMA$_2$ used at concentration between 10 and 30 ng/µL (Fig. 10C). The positive control tested 40 ± 1 PFU/mL in the plaque assay. MISMA$_2$ reduced the formation of plaques to 4 ± 2, 8 ± 1 and 13 ± 1 PFU/mL when used at 10, 20 and 30 ng/µL, respectively, which corresponded to 90 ± 0.9, 80 ± 0.1 and 66 ± 0.5 % of inhibition ($p = 0.0022$, Mann-Whitney test). Of note is the fact that these MISMAs dilutions were not toxic to the cells (Fig. 10D) as revealed by the levels of Crystal Violet staining as indicator of the live cells attached to the wells.

In the attempt to figure out the lack of virucidal activity of MISMA$_2$ at concentrations above 100 ng/µL, the particle size distribution of MISMA$_2$ at the two limit concentrations was studied by NTA before and after storage for 15 h at 37°C. As exemplified in Fig. 11, MISMA$_2$ clearly showed a tendency to self-aggregate at high concentration values since the signal of single nanoparticle was not visible anymore in both experimental conditions (Fig. 11B). The modification of the particle size and structure of MISMA$_2$ might be responsible for the loss of efficacy in recognizing the RBD and, thus, in exerting a virucidal activity.

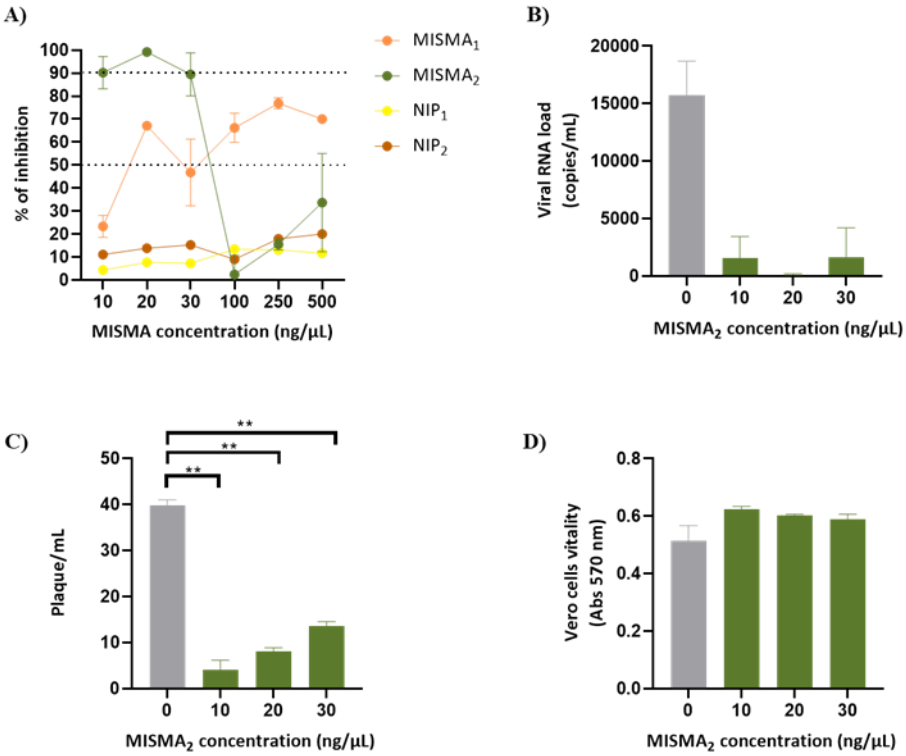

Figure 10. MISMAs inhibition activity on in vitro SARS-CoV-2 infectivity. PANEL A: Inhibition of viral replication in Vero cells by MISMA$_1$ and MISMA$_2$ measured as reduction of viral load in culture supernatant. Dotted lines indicate 50 and 90% inhibition of viral transmission. **PANEL B:** Viral production as detected by RT-PCR in presence and absence of MISMA$_2$. The mean and SD of triplicates from one experiment is shown. **PANEL C:** Inhibition of SARS-CoV-2 replication as measured by a plaque assay on Vero cells. The mean and SD of triplicates from two independent experiments is shown. ** indicate $p < 0.005$ as calculated with Mann-Whitney test. **PANEL D:** Cell vitality measured by Crystal Violet assay performed in Vero cells treated with MISMA$_2$. The mean OD (optical density) values and SD of one representative experiment performed in triplicate is shown.

ARTICLE

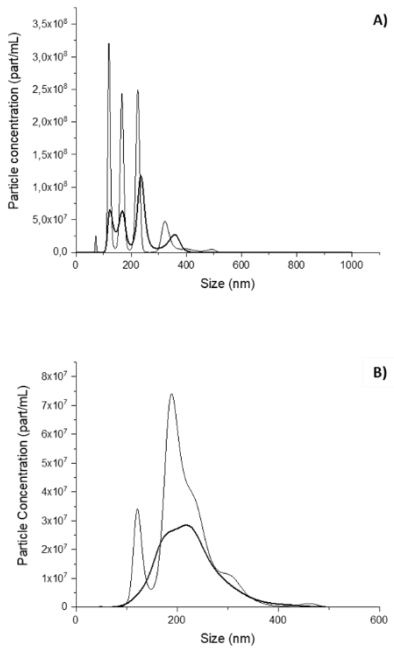

Figure 11. NTA traces of MISMA$_2$ at time 0 (thin line) and after 15 h storage at 37°C (thick line). Two different concentrations corresponding to the lowest (**Panel A**) and highest (**Panel B**) one used in *in vitro* experiments are shown.

Experimental section

Reagents

Receptor-Binding Domain of SARS-CoV-2 (2019-nCoV) Spike Protein (RBD, mFc Tag) and Receptor-Binding Domain of Human SARS Coronavirus Spike Protein (RBD, His Tag) were purchased from Sino Biological Inc. (Beijing, China).

Acrylamide (AAm), acrylic acid (AA), N,N'-methylenebisacrylamide (BIS), tween-80, span-80, dioctyl sulfosuccinate sodium salt (AOT), ammonium persulfate (APS), N,N,N,N-tetramethylethylenediamine (TEMED), disodium hydrogen phosphate, sodium dihydrogen phosphate, sodium dodecyl sulfate (SDS), acrylamide/bis-acrylamide solution (A3449), tris(hydroxymethyl)aminomethane-HCl(Tris-HCl), bromophenol blue, 2-mercaptoethanol, glycerol, glacial acetic acid, formic acid, Coomassie Brilliant blue R, Hepes buffer, crystal violet, bovine serum albumin (BSA), TBS (20 mM Tris-HCl, 150 mM NaCl, pH 7.5), TBS-T (0.05% Tween 20 in TBS) were purchased from Sigma-Aldrich s.r.l. (Milan, Italy).

The ACE2:Spike RBD (SARS-CoV-2) Inhibitor Screening Assay Kit (Catalog number 79936) was obtained by BPS Bioscience (San Diego, CA, USA).

All solvents were reagent or HPLC grade and obtained from VWR (Milan, Italy).

Dulbecco's Modified Eagle Medium (DMEM), Fetal Calf Serum (FCS), Penicillin/Streptomycin 100X, Agarose were purchased from Euroclone (Pero, Italy).

Ag-Path one-step RT-PCR was purchased from Lifetechnologies (Carlsbad, CA, USA).

Primers and probe for RT-PCR were purchased from Eurofins genomics (Ebersberg, Germany).

Formaldehyde was purchased from Applichem (Darmstadt, Germany).

Methylene Blue was purchased from Merck (Darmstadt, Germany).

Nucleospin RNA virus kit was purchased from Macherey-Nagel (Duren, Germany).

Instrumentation

The TEM micrographs were obtained using a Jeol Transmission Electron Microscope, model JEM-1409Plus, operating at 80 Kv power.

The particle size distribution was determined both by dynamic light scattering (DLS), using a Zetasizer (Nano-ZS, Malvern Instrument, UK), and Nanoparticle Trafficking Analysis (NTA) using a Nanosight NS 300 (Malvern Instrument, UK). In the first case, particle size measurements were carried out inserting the sample dispersed in Hepes buffer 20 mM in a disposable cuvette with a detection angle of 173°.

ζ-potential was assessed on the samples inserted in a capillary cell. Three measurements were taken for each sample and the results are expressed as the mean and standard deviation. For NTA analysis, the samples properly diluted in Hepes buffer (0.01 micron) underwent 6 sequential measurements at 25°C using a Blue488 laser.

Absorption spectra were recorded with a Jasco V-530 UV/Vis spectrometer.

A Synergy H1 Hybrid Reader (BioTek, USA) was used to measure the chemiluminescence and for the crystal violet assay.

The dot-blot analysis was performed using an iBright FL1500 Imaging System (ThermoFisher Scientific, USA).

HPLC was performed using a Varian 900-LC (Varian Inc., California, UK) equipped with an autosampler, a quaternary pump and a fluorescence detector set at an excitation wavelength of 274 nm and an emission wavelength of 304 nm. A 250 × 4.6 mm C-18 Viva™ column, particle size 5 µm (Restek, Barcelona, Spain) was employed. The flow rate was 1.0 mL/min and injection volume was 30 µL. The mobile phase was a 10:90 (v/v) mixture of HPLC-grade water containing 0.8% formic acid and acetonitrile containing 0.7% formic acid. HPLC data were acquired using Galaxie™ Chromatography Software. The adopted HPLC conditions for peptides analysis have been previously reported in literature with slight modification.[47]

RT-Real Time PCR was performed using the 7500 Gene Systems (Applied Biosystems, USA).

SDS-PAGE Electrophoresis

SDS-PAGE electrophoresis was performed on 14% gels and a SARS-CoV-2 receptor-binding domain (RBD) solution in PBS at pH 7.4 was used as control. 30 µL of each sample (RBD standard solution and the supernatants obtained from binding experiments for MISMAs and NIPs) were loaded in each well. Gel electrophoresis was performed in Mini Protean Tetra Cell Apparatus (Bio-Rad Laboratories, USA). After sample loading, electrophoresis was performed at 80 to 100 volts. Gels were stained by Coomassie Brilliant Blue R-250. After destaining, the gels were stored in gel storage solution and photographed.

Computational Methods and Analysis

SARS-CoV-2 RBD structure was retrieved from Brookhaven Protein Data Bank (Uniprot P00374, pdb code 6w41, 7m0j) (http://www.wwpdb.org), processed within the CHIMERA software,[48] and minimized using AMBERff14 force field within AMBER 2018 suite;[49] a progressive minimization was carried out until the average root mean square deviation (RMSD) of the non-hydrogen atoms reached 0.3 Å and the resulting structure was then used in molecular docking calculations. Acrylamide structure was built in and minimized using Gaussian16 at DFT/6-311G* level of theory (PubChem CID: 6579);[50] the same protocol has been applied to acrylic acid and its conjugate anion, acrylate (PubChem CID: 6581).

Autodock 4.2/MGLTools5.4 was used to perform the molecular docking calculations[51] using the previously calculated charges at QM/DFT level for the ligands. Particularly, we tested the cluster distribution considering different charges types (i.e. Mulliken, NBO), obtaining in the two cases a high correspondence of the clusters' distribution. Initially, a blind docking approach was used in order to identify every putative site on the RBD surface. To predict the probable arrangement of multiple monomer molecules around the protein, a detailed cluster analysis was performed and clusters that fall within the contact surfaces between monomeric chains in the trimeric association of the spike protein were excluded from further analysis. Subsequently, on the lowest energy and most populated poses, a focused docking protocol has been applied to better refine both pose and its energy. For the Blind docking, the grid map, cantered in the center of mass of the enzyme (126x126x126 Å3) included all the RBD surface; in the focused docking protocol, the grid map was centred on the ligand in the considered pose and extended around the cleft (40x40x40 Å3) with points spaced equally at 0.375 Å. The number of GA (genetic algorithm) runs was set to 150, the energy evaluations (25 000 000), the maximum number of top individuals that automatically survive (0.1) and the step size for translation (0.2 Å). All the docking calculations were carried out in triplicate using three different CPUs random seed. The final docked RBD-acrylamide complexes were ranked according to the predicted binding energy and all the conformations were processed using the built-in clustering analysis with a 2.0 Å cut-off. The same protocol was applied to predict acrylic acid/acrylate binding sites and scoring. The final structures were minimized using AM-BERff14 force field within AMBER18 software package.[49, 52]

Synthesis of Molecularly Imprinted Synthetic Material Antibodies (MISMAs)

Molecularly Imprinted Synthetic Material Antibodies (MISMAs) were prepared by inverse microemulsion polymerization. Two different materials were synthesized according to the compositions reported in Table 5.

The water phase was prepared in a vial dissolving functional and crosslinking monomers in 1.0 mL of distilled water and sonicating for 3 min. Then, SARS-CoV-2 receptor-binding domain was added to the obtained solution, which was agitated for 1 h at room temperature to promote the formation of the template-monomer pre-polymerization complex. For the preparation of the oil phase, deoxygenated hexane (22 mL), AOT (0.8 g), Span-80 (0.87 mL) and Tween-80 (0.68 mL) were mixed together. Then, the aqueous phase was added dropwise into the hexane solution and stirred vigorously at room temperature in order to form the microemulsion. After 1 h, the polymerization was initiated at room temperature by adding APS (40 mg) and TEMED (100 µL) and the reaction mixture was left under stirring for 2 h.

The obtained polymeric nanoparticles were precipitated with ethanol (40 mL) and collected by centrifugation at 6,000 rpm for 30 min. In order to remove unreacted components, surfactants and template, the nanoparticles were washed with acetic acid (10% v/v in water), water, ethanol, acetone and, finally, diethyl ether. At the end, the polymeric material was dried overnight.[42, 43]

Non-Imprinted Polymers (NIPs) were also synthesized following the same experimental conditions, but in the absence of the template.

Binding Studies

The binding experiments were carried out mixing 5 mg of the imprinted and non-imprinted nanoparticles with 0.5 mL of PBS at pH 7.4 (10^{-3} M) and 0.5 mL of a SARS-CoV-2 RBD standard solution (20 µg/mL in PBS at pH 7.4). After 18 h, each sample was centrifuged at 13,000 rpm for 15 min and the RBD amount in the supernatants was determined by SDS-page electrophoresis.

In order to investigate the selectivity of the synthesized imprinted nanoparticles, non-competitive binding studies were also performed in the presence of SARS-CoV receptor-binding domain as structural analogue according to the same experimental protocol.

The experiments were carried out in triplicate.

Table 5. Composition of the polymerization mixture.

POLYMER	RBD (µg)	AAm (g)	AA (g)	BIS (g)
MISMA₁	100	0.45	-	0.13
NIP₁	-	0.45	-	0.13
MISMA₂	100	0.40	0.045	0.13
NIP₂	-	0.40	0.045	0.13

Dot- blot Assay

A dot-blot assay was performed in the aim to further investigate the ability of the prepared MISMAs to bind the receptor-binding domain of SARS-CoV-2. For this purpose, $MISMA_2$, which provided the best results in terms of binding properties, and the corresponding non-imprinted polymer were previously loaded with rhodamine 6G as fluorescent probe. Then, 10 mg of the imprinted and non-imprinted polymeric nanoparticles were dispersed in 1.0 mL of a $2x10^{-4}$ M rhodamine solution in distilled water. After 24 h incubation, polymeric nanoparticles were recovered by centrifugation at 13,000 rpm for 10 min, washed several times with ethanol to remove unloaded rhodamine and, finally, dried.
For dot-blot analysis, different amounts of SARS-CoV-2 RBD (250, 200, 100, 50, 25, 10, 1 and 0.5 ng) were spotted on two nitrocellulose membranes (Nitrocellulose Membrane, 0.45 μm, #1620148, Bio-Rad Laboratories, Inc.). Membranes were dried and, then, blocked by soaking in 5% BSA in TBS-T in a Petri dish for 1 h at room temperature. After being washed three times with TBS-T, the membranes were incubated overnight with imprinted or non-imprinted polymeric nanoparticles (100 ng/mL). After washing as before, the images were captured.
The same experimental protocol was carried out using SARS-CoV receptor-binding domain as structural analogue of SARS-CoV-2 RBD.

Static Equilibrium Adsorption Experiments

Adsorption isotherms studies allow to better investigate the interaction between the template molecule and the imprinted nanoparticles. Therefore, in the aim to obtain more information about the nature of this interaction, further binding experiments were performed on $MISMA_2$ as reported before, but using SARS-CoV-2 RBD standard solutions at different concentrations (1-60 μg/mL in PBS at pH 7.4).
The binding experiments were repeated in triplicate.

ACE2:Spike RBD (SARS-CoV-2) Inhibitor Screening Assay

The ability of the prepared MISMAs to inhibit the interaction between ACE2 and the receptor-binding domain of SARS-CoV-2 was investigated using the ACE2:SARS-CoV-2 Spike RBD Inhibitor Screening Assay Kit according to the manufacturer's instructions.
The first step of the performed assay involved the anchorage of ACE2 protein to a nickel-coated 96-well plate and, then, SARS-CoV-2 Spike Protein (RBD) mFc Tag was incubated with ACE2 on the plate in the presence of imprinted or non-imprinted polymeric nanoparticles, which were tested at different concentrations in the range from 0.1 to 50 ng/μL. The plate was treated with anti-mouse-Fc-HRP followed by addition of an HRP substrate to produce chemiluminescence. Blank value was subtracted from all readings.

Cells and Virus

Vero cells (African green monkey Kidney Epithelial Cells, ATCC CCL81) were purchased from ATCC (Manassas, VA, USA) and maintained in DMEM medium supplemented with 10% heat-inactivated fetal calf serum (FCS), 2 mM glutamine, 100 units/mL of penicillin, 100 μg/mL of streptomycin and were used to test the antiviral activity of MISMAs.
The SARS-CoV-2/UNIMI-1 strain (accession number GenBank MT748758, GISAID EPI_ISL 584051) was previously isolated at the Laboratory of Molecular Virology, University of Milano, Italy, from a COVID-19 patient's oropharyngeal swab, and was used for the infection experiments.

Anti SARS-CoV-2 Inhibition Assay

Vero cells were seeded into 96-well plates at a density of 1.3×10^4 cells/well in DMEM with 10% FCS and 1x Penicillin/Streptomicin, and were incubated for 24 hours at 37°C, 5% CO_2. The virus, used at a multiplicity of infection (MOI) of 0.01, was incubated for 1 h at 37°C with imprinted and non-imprinted polymeric nanoparticles (10, 20, 30, 100, 250, 500 ng/μL) and, then, added to the cell monolayer for 2 hours at 37°C, 5% CO_2. After removal of the virus inoculum, cells were incubated for 72 hours at 37°C, 5% CO_2.
At the end of the infection, the culture supernatant was collected and viral RNA was isolated using the Nucleospin RNA virus kit (Macherey-Nagel, Germany), following the manufacturer's protocol. Quantification of viral copy numbers in the cell supernatant was evaluated via specific qRT-PCR, targeting the N1 gene, as previously described,[53] using the 7500 Gene Systems (Applied Biosystems, USA). A standard curve was created using a plasmid containing the complete SARS-CoV-2 genome, using 10-fold dilutions from 10^8 to 10^0.
The experiments were conducted in triplicate.

Sars-CoV-2 Plaque Assay of *in vitro* Virus Replication

Vero cells were seeded at 7.5 x 10^5 cells/well in 6 well plates in DMEM with 10% FCS and 1x Penicillin/Streptomicin; 24h later 100 plate forming unit/mL (PFU/mL) of a previously titrated SARS-CoV-2 isolate were added to $MISMA_2$ (from 30 to 10 ng/μL) serially diluted in DMEM, and incubated for 1h before addition to confluent Vero cells. Cells supernatants were discarded after 2h, and 0.3% agarose (3 μg/mL) dissolved in DMEM was added to each well. After 72 hours, cells were fixed with 4% formaldehyde solution and, upon agarose removal, stained with methylene blue (0.4 g/L). Viral plaques were counted, and results were expressed as Plaque Forming Unit (PFU)/mL. Each condition was performed in triplicate and the experiment was repeated twice.

Cytotoxicity

Crystal Violet assay was employed to define MISMAs cytotoxicity. Briefly, Vero cells were seeded into 96-well plates at a density of 1.3×10^4 cells/well in DMEM with 10% FCS and 1x Penicillin/Streptomicin, and were incubated for 24 hours at 37°C, 5% CO_2. $MISMA_2$ (10, 20 and 30 ng/μL) was added to the cell monolayer for 72 hours at 37°C, 5% CO_2. Then, cell medium was removed, cells were washed with PBS, and fixed with 200 μL of 0.5% Crystal Violet (0.25 g in 50 mL 4% formaldehyde) for 30 minutes. Solubilization solution (200 μL methanol) was added for 30 minutes before the analysis, performed using a microplate reader at 570 nm absorbance.

Data Visualization and Statistical Analysis

Statistics analysis were performed using GraphPad Prism version 8.1 software (GraphPad Software, La Jolla, USA).
Two-way ANOVA followed by Šídák's multiple comparison test was used to analyze data from the ACE2:Spike RBD (SARS-CoV-2) Inhibitor

Screening Assay. P values of 0.05 or lower were considered significant, *p < 0.05, **p < 0.01, ***p < 0.001 and ****p < 0.0001. The non-parametric Mann Whitney was used to compare the infectivity of the virus in the inhibition assay. P values of 0.05 or lower were considered significant, *p < 0.05, **p < 0.01.

Conclusions

In the present study, Molecular Imprinting Technology was adopted as a strategy for the synthesis of a Molecularly Imprinted Polymer able to selectively recognize and bind the spike protein RBD of the novel coronavirus SARS-CoV-2. The results we reported here confirmed the ability of the synthesized nanoparticles to significantly exert an antiviral activity *in vitro*, suggesting their potential use as MIP-based plastic antibodies devoted to block the function of the viral spike protein. These results support their use as effective alternative to the expensive traditional antibodies often unreliable due to their restricted stability.

MIPs-based antibodies could be administered parenterally, but different formulation possibilities and alternative routes could be also considered. Aerosol represents one of the main procedures for the treatment of pulmonary diseases at home and healthcare setting, while nasal and throat sprays allow to deliver therapeutic agents both locally and systemically throughout nasal and oral mucosa, respectively.

Given these characteristics, the developed nanoparticles could be potentially used as free-drug therapeutics in the prevention and treatment of SARS-CoV-2 infection. Moreover, if used in combination with antiviral agents, these nanoparticles could act as a powerful multimodal system combining their ability to block the viral spike protein with the targeted delivery of the loaded drug. In addition, the same nanoparticles can be further engineered to become a MIP-based sensor for diagnostic purpose.

Author Contributions

Project Administration, F.P.*; Conceptualization, Supervision and Data Curation, F.P.*, O.I.P. and V.P.; Writing, O.I.P.; Methodology and Formal Analysis, M.D., R.M., F.P. and M.R.; *in vitro* studies on SARS-CoV-2, S.D., P.F., S.P. and M.C.; Docking Studies R.G.; DLS and NTA analyses, F.C., S.F. and F.S.; TEM analyses, I.P.

Conflicts of interest

There are no conflicts to declare.

Acknowledgements

This work was supported by University of Calabria and Macrofarm s.r.l., a spin-off company of the University of Calabria.

Notes and references

1. P. Zhou, X.-L. Yang, X.-G. Wang, B. Hu, L. Zhang, W. Zhang, H.-R. Si, Y. Zhu, B. Li and C.-L. Huang, *Nature*, 2020, **579**, 270-273.
2. World Health Organization, WHO Coronavirus (COVID-19) Dashboard, https://covid19.who.int, (accessed June, 2021).
3. G. Lu, Q. Wang and G. F. Gao, *Trends Microbiol.*, 2015, **23**, 468-478.
4. Q. Wang, G. Wong, G. Lu, J. Yan and G. F. Gao, *Antivir. Res.*, 2016, **133**, 165-177.
5. R. Lu, X. Zhao, J. Li, P. Niu, B. Yang, H. Wu, W. Wang, H. Song, B. Huang and N. Zhu, *Lancet*, 2020, **395**, 565-574.
6. F. Li, W. Li, M. Farzan and S. C. Harrison, *Science*, 2005, **309**, 1864-1868.
7. Y. Wan, J. Shang, R. Graham, R. S. Baric and F. Li, *J. Virol.*, 2020, **94**.
8. X. Xu, P. Chen, J. Wang, J. Feng, H. Zhou, X. Li, W. Zhong and P. Hao, *Sci. China Life Sci.*, 2020, **63**, 457-460.
9. C. Lei, K. Qian, T. Li, S. Zhang, W. Fu, M. Ding and S. Hu, *Nat. Commun.*, 2020, **11**, 1-5.
10. R. Yan, Y. Zhang, Y. Li, L. Xia, Y. Guo and Q. Zhou, *Science*, 2020, **367**, 1444-1448.
11. Food & Drug Administration, Learn More About COVID-19 Vaccines From the FDA, https://www.fda.gov/consumers/consumer-updates/learn-more-about-covid-19-vaccines-fda, (accessed June, 2021).
12. Food & Drug Administration, Pfizer-BioNTech COVID-19 Vaccine, https://www.fda.gov/emergency-preparedness-and-response/coronavirus-disease-2019-covid-19/pfizer-biontech-covid-19-vaccine, (accessed April, 2021).
13. Food & Drug Administration, FDA Takes Additional Action in Fight Against COVID-19 By Issuing Emergency Use Authorization for Second COVID-19 Vaccine, https://www.fda.gov/news-events/press-announcements/fda-takes-additional-action-fight-against-covid-19-issuing-emergency-use-authorization-second-covid, (accessed April, 2021).
14. Food & Drug Administration, FDA Issues Emergency Use Authorization for Third COVID-19 Vaccine, https://www.fda.gov/news-events/press-announcements/fda-issues-emergency-use-authorization-third-covid-19-vaccine, (accessed June, 2021).
15. R. K. Guy, R. S. DiPaola, F. Romanelli and R. E. Dutch, *Science*, 2020, **368**, 829-830.
16. S. Drożdżal, J. Rosik, K. Lechowicz, F. Machaj, K. Kotfis, S. Ghavami and M. J. Łos, *Drug Resist. Updat.*, 2020, **53**, 100719.
17. C. Wang, W. Li, D. Drabek, N. M. Okba, R. van Haperen, A. D. Osterhaus, F. J. van Kuppeveld, B. L. Haagmans, F. Grosveld and B.-J. Bosch, *Nat. Commun.*, 2020, **11**, 1-6.
18. Food & Drug Administration, Coronavirus Treatment Acceleration Program (CTAP), https://www.fda.gov/drugs/coronavirus-covid-19-drugs/coronavirus-treatment-acceleration-program-ctap, (accessed June, 2021).
19. Food & Drug Administration, Emergency Use Authorization, https://www.fda.gov/emergency-preparedness-and-response/mcm-legal-regulatory-and-

policy-framework/emergency-use-authorization#coviddrugs, (accessed April, 2021).
20. P. Chames, M. Van Regenmortel, E. Weiss and D. Baty, *Br. J. Pharmacol.*, 2009, **157**, 220-233.
21. D. Refaat, M. G. Aggour, A. A. Farghali, R. Mahajan, J. G. Wiklander, I. A. Nicholls and S. A. Piletsky, *Int. J. Mol. Sci.*, 2019, **20**, 6304.
22. J. Xu, H. Miao, J. Wang and G. Pan, *Small*, 2020, **16**, 1906644.
23. J. Pan, W. Chen, Y. Ma and G. Pan, *Chem. Soc. Rev.*, 2018, **47**, 5574-5587.
24. O. I. Parisi, C. Morelli, F. Puoci, C. Saturnino, A. Caruso, D. Sisci, G. E. Trombino, N. Picci and M. S. Sinicropi, *J. Mater. Chem. B*, 2014, **2**, 6619-6625.
25. O. I. Parisi, M. Ruffo, R. Malivindi, A. F. Vattimo, V. Pezzi and F. Puoci, *Pharmaceutics*, 2020, **12**, 41.
26. A. M. Piloto, D. S. Ribeiro, S. S. M. Rodrigues, C. Santos, J. L. Santos and M. G. F. Sales, *Sci. Rep.*, 2018, **8**, 1-11.
27. M. Wubulikasimu, T. Muhammad, M. Imerhasan, N. Hudaberdi, W. Yang, J. Zhao and X. Peng, *RSC Adv.*, 2019, **9**, 6779-6784.
28. A. Capriotti, S. Piovesana, R. Z. Chiozzi, C. M. Montone, A. M. Bossi and A. Laganà, *J. Proteom.*, 2020, **219**, 103736.
29. K. Haupt, P. X. Medina Rangel and B. T. S. Bui, *Chem. Rev.*, 2020, **120**, 9554-9582.
30. P. X. Medina Rangel, E. Moroni, F. Merlier, L. A. Gheber, R. Vago, B. Tse Sum Bui and K. Haupt, *Angew. Chem. Int. Ed.*, 2020, **59**, 2816-2822.
31. Y. Dong, W. Li, Z. Gu, R. Xing, Y. Ma, Q. Zhang and Z. Liu, *Angew. Chem. Int. Ed.*, 2019, **58**, 10621-10625.
32. F. Cui, Z. Zhou and H. S. Zhou, *Sensors*, 2020, **20**, 996.
33. M. Dinc, C. Esen and B. Mizaikoff, *Trends Analyt. Chem.*, 2019, **114**, 202-217.
34. S. P. Graham, H. F. El-Sharif, S. Hussain, R. Fruengel, R. K. McLean, P. C. Hawes, M. V. Sullivan and S. M. Reddy, *Front. Bioeng. Biotechnol.*, 2019, **7**, 115.
35. J. Lan, J. Ge, J. Yu, S. Shan, H. Zhou, S. Fan, Q. Zhang, X. Shi, Q. Wang and L. Zhang, *Nature*, 2020, **581**, 215-220.
36. X. Wang, S. Yu, J. Wang, J. Yu, M. Arabi, L. Fu, B. Li, J. Li and L. Chen, *Talanta*, 2020, **211**, 120727.
37. S. Resende, M. F. Frasco and M. G. F. Sales, *Sens. Actuators B Chem.*, 2020, **312**, 127947.
38. W. Zhao, B. Li, S. Xu, Y. Zhu and X. Liu, *Anal. Chim. Acta*, 2020, **1117**, 25-34.
39. L. Luo, J. Yang, K. Liang, C. Chen, X. Chen and C. Cai, *Talanta*, 2019, **202**, 21-26.
40. L. Luo, F. Zhang, C. Chen and C. Cai, *Microchim. Acta*, 2020, **187**, 140.
41. J. Xu, F. Merlier, B. Avalle, V. Vieillard, P. Debré, K. Haupt and B. Tse Sum Bui, *ACS Appl. Mater. Interfaces*, 2019, **11**, 9824-9831.
42. Y. Zhang, C. Deng, S. Liu, J. Wu, Z. Chen, C. Li and W. Lu, *Angewa. Chem.*, 2015, **127**, 5246-5249.
43. Z. Wu, J. Hou, Y. Wang, M. Chai, Y. Xiong, W. Lu and J. Pan, *Int. J. Pharm.*, 2015, **496**, 1006-1014.
44. O. I. Parisi, M. Ruffo and F. Puoci, in *Nanostructured Biomaterials for Regenerative Medicine*, eds. V. Guarino, M. Iafisco and S. Spriano, Elsevier, 2020, ch. 5, pp. 141-163.
45. R. Viveiros, M. I. Lopes, W. Heggie and T. Casimiro, *Chemical Engineering Journal*, 2017, **308**, 229-239.
46. H. Wang, L. Yuan, H. Zhu, R. Jin and J. Xing, *Journal of Polymer Science Part A: Polymer Chemistry*, 2019, **57**, 157-164.
47. S. Saraswat, B. Snyder and D. Isailovic, *Journal of Chromatography B*, 2012, **902**, 70-77.
48. E. F. Pettersen, T. D. Goddard, C. C. Huang, G. S. Couch, D. M. Greenblatt, E. C. Meng and T. E. Ferrin, *J. Comput. Chem.*, 2004, **25**, 1605-1612.
49. K. B. D.A. Case, I.Y. Ben-Shalom, S.R. Brozell, D.S. Cerutti, T.E. Cheatham, III, V.W.D. Cruzeiro, T.A. Darden, R.E. Duke, G. Giambasu, M.K. Gilson, H. Gohlke, A.W. Goetz, R. Harris, S. Izadi, S.A. Izmailov, K. Kasavajhala, A. Kovalenko, R. Krasny, T. Kurtzman, T.S. Lee, S. LeGrand, P. Li, C. Lin, J. Liu, T. Luchko, R. Luo, V. Man, K.M. Merz, Y. Miao, O. Mikhailovskii, G. Monard, H. Nguyen, A. Onufriev, F.Pan, S. Pantano, R. Qi, D.R. Roe, A. Roitberg, C. Sagui, S. Schott-Verdugo, J. Shen, C.L. Simmerling, N.R. Skrynnikov, J. Smith, J. Swails, R.C. Walker, J. Wang, L. Wilson, R.M. Wolf, X. Wu, Y. Xiong, Y. Xue, D.M. York and P.A. Kollman, AMBER18, University of California, San Francisco, 2018.
50. G. W. T. M. J. Frisch, H. B. Schlegel, G. E. Scuseria, M. A. Robb, J. R. Cheeseman, G. Scalmani, V. Barone, G. A. Petersson, H. Nakatsuji, X. Li, M. Caricato, A. V. Marenich, J. Bloino, B. G. Janesko, R. Gomperts, B. Mennucci, H. P. Hratchian, J. V. Ortiz, A. F. Izmaylov, J. L. Sonnenberg, D. Williams-Young, F. Ding, F. Lipparini, F. Egidi, J. Goings, B. Peng, A. Petrone, T. Henderson, D. Ranasinghe, V. G. Zakrzewski, J. Gao, N. Rega, G. Zheng, W. Liang, M. Hada, M. Ehara, K. Toyota, R. Fukuda, J. Hasegawa, M. Ishida, T. Nakajima, Y. Honda, O. Kitao, H. Nakai, T. Vreven, K. Throssell, J. A. Montgomery, Jr., J. E. Peralta, F. Ogliaro, M. J. Bearpark, J. J. Heyd, E. N. Brothers, K. N. Kudin, V. N. Staroverov, T. A. Keith, R. Kobayashi, J. Normand, K. Raghavachari, A. P. Rendell, J. C. Burant, S. S. Iyengar, J. Tomasi, M. Cossi, J. M. Millam, M. Klene, C. Adamo, R. Cammi, J. W. Ochterski, R. L. Martin, K. Morokuma, O. Farkas, J. B. Foresman, and D. J. Fox, GAUSSIAN 16 (Revision C.01), Gaussian Inc., Wallingford, CT, 2016.
51. G. M. Morris, R. Huey, W. Lindstrom, M. F. Sanner, R. K. Belew, D. S. Goodsell and A. J. Olson, *J. Comput. Chem.*, 2009, **30**, 2785-2791.
52. J. A. Maier, C. Martinez, K. Kasavajhala, L. Wickstrom, K. E. Hauser and C. Simmerling, *J. Chem. Theory Comput.*, 2015, **11**, 3696-3713.
53. World Health Organization, WHO. Coronavirus disease (COVID-19) technical guidance: Laboratory testing for 2019-nCoV in humans. US CDC Real-time RT-PCR Panel for Detection 2019-Novel Coronavirus, https://www.fda.gov/media/134922/download (accessed January, 2020).